JOURNAL OF GEOPHYSICAL RESEARCH, VOL. 104, NO. A3, 4669–4680, DOI:10.1029/1998JA900157, 1999

Electromagnetic ion beam instabilities: Oblique pulsations

P. Hellinger

Institute of Atmospheric Physics, Prague, Czech Republic

A. Mangeney

Observatory of Paris, Meudon, France

Abstract. We present results of a two-dimensional hybrid simulation of the electromagnetic proton beam instability. We show that for a case of cold and rather high density proton beam the oblique right-handed resonant modes play an important role. The interaction of these modes with the beam protons causes significant beam density fluctuations. At the nonlinear stage the oblique modes give rise to a beam filamentation. Beam filaments influence strongly the evolution of the instability. They create pulses of a strong magnetic field. These pulses share some properties of the magnetic pulsations (short, large-amplitude magnetic structures). We suppose that the oblique modes play an important role in the structure of the quasi-parallel Earth's bow shock.

1. Introduction

The terrestrial foreshock is a very complex region with a high level of electromagnetic fluctuations and strongly nonthermal ion distribution functions, with beams of particles coming from the bow shock [*Tsurutani and Stone*, 1985]. Understanding the physics of the interaction between waves and particles in the foreshock is a complicated task because of the combination of significant nonlinearities and inhomogeneities combined with the fact that, usually, the waves are transported by the solar wind out of the region of generation toward the shock. A considerable amount of theoretical work has been done to understand the basic properties of the beam-plasma system in the foreshock context, using linear and quasi-linear theories as well as numerical simulations; see the review of *Gary* [1991, and references within].

Since the upstream beams and waves are intimately connected with the bow shock itself, realistic simulations of the full shock structure would be desirable but are, at the moment, beyond the reach of today's computational facilities, since the typical scales (both spatial and temporal) of the shock are much greater than the proton scales typical of kinetic (hybrid or particle) simulations. On the other hand, many simulations of the quasi-perpendicular or quasi-parallel portion of the bow shock have been done. These simulations have helped in understanding the shock structure; the quasi-perpendicular shocks are now very well understood, but this is not the case for quasi-parallel shock waves. The simulations of quasi-parallel shocks show a general feature, namely that the shock structure is not stable, but it reforms itself [see *Burgess*, 1989].

However, the simulation does not reproduce an important structure of the shock, the magnetic pulsations. This is probably because the simulations did not run long enough to have the upstream turbulence fully developed (for discussion, see *Scholer* [1993]); more realistic simulations are, however, very expensive.

At the level of linear theory, two important results have been established. The first one is that ion-ion electromagnetic instabilities (with frequencies and growth rates of the order or less then the ion gyrofrequency) are generally the most robust ones and may grow to higher amplitudes than the ion-electron electromagnetic and electrostatic instabilities, even if the latter have generally higher growth rates.

The second result is that the behavior of the beam-plasma system is quite sensitive to the beam properties. For a high-temperature beam with a small drift velocity the most unstable mode is a left-handed resonant (LHR) mode; if the drift velocity is sufficiently high, it is a right-handed resonant (RHR) mode for a cold, low-density beam and a left-handed nonresonant (LHN) mode for a high-density and/or temperature beam. In all cases, however, the maximum growth rates are found for (anti)parallel propagation with respect to the ambient magnetic field.

These predictions of linear theory are in good agreement with the properties of the weak amplitude, $\delta B/B_0 < 1$ (where B_0 is the amplitude of the ambient magnetic field), almost monochromatic ULF waves found close to the proton foreshock boundary. The observed wave properties that are right-handed in the plasma frame and propagate parallel to the ambient magnetic field are consistent with those of the RHR instability driven by field-aligned back-streaming protons, reflected off the oblique portion of the Earth's bow shock. Moreover, the numerical simulations by *Winske and Leroy* [1984] show that the nonlinear evolution of the distribution function in the case of the RHR instability is consistent with the observations of a gradual modification of the velocity distribution of back-streaming protons from "reflected" type toward "intermediate" type.

However, deeper into the proton foreshock, the situation is far from being well understood. The electromagnetic fluctuations can reach rather large amplitudes, $\delta B/B_0 \sim 1$, for "shocklets," which are compressible, right-handed (in the plasma frame), periodic, but nonsinusoidal wave trains, and, still higher, $\delta B/B_0 \sim 3-4$ for "pulsations" (or short, large-amplitude magnetic structures (SLAMS)), which are mostly left-handed (in the plasma frame), compressible, localized perturbations [*Thomsen et al.*, 1990; *Schwartz et al.*, 1992; *Mann et al.*, 1994]. Very strong evidence of nonlinear behavior has been provided by the statistical analysis of shocklets [see, e.g., *Elaoufir et al.*, 1990] and SLAMS [*Mann et al.*, 1994], and these two types of perturbations propagate obliquely with respect to the ambient magnetic field.

Are these structures the result of the nonlinear evolution, combined with transport by the flow, of initially parallel propagating unstable waves, as one would expect from linear theory? In that case, what is the mechanism that causes the waves to "refract" from parallel to oblique propagation? The case of pulsations appears to be more complicated than the case of shocklets; they both seem to grow out from the ULF waves, but they have a different polarization and propagation angle.

Some authors have attempted to follow these ULF waves in the nonlinear regime; for example, *Akimoto et al.* [1991, 1993] have studied the case of RHR and LHN parallel propagating waves generated by cold ion beams in one-dimensional (1-D) hybrid simulations. They have shown that both the modes end up in magnetic pulsations that share some similarities with the observed ones. However, such simulations miss the important observational fact that the observed perturbations propagate obliquely.

0148-0227/05/1998JA900157$9.00

Table 1. Plasma Parameters for Linear theory, and the Hybrid Simulation

Plasma parameters		
$\omega_{pe}/\Omega_e = 200$	$\beta_e = \beta_p = 0.5$	$T_b = T_p$
$v_b = 10 v_A$	$n_b/n_p = 0.04$	

Since the properties of the beams are expected to vary as the shock normal goes from oblique to quasi-parallel, as well as with increasing distance from the shock front, a possible interpretation of the observed oblique propagation of the perturbations is that these inhomogeneities can refract the initially parallel propagating waves [*Hada et al.*, 1987], which may then grow and evolve as the oblique modes in the numerical study by *Omidi and Winske* [1990] and become shocklets. Simultaneously, the intermediate back-streaming protons will be scattered and end up in the diffuse state.

However, this scenario does not account for the recent observations by *Fuselier et al.* [1995] [see also *Ipavich et al.*, 1988], who show that the abundance of suprathermal He^{2+} found in conjunction with the diffused back-streaming protons is not consistent with that found with either the field-aligned or intermediate beams. Thus there is no evolution sequence from reflected to diffuse ions; the diffuse protons are originating from the quasi-parallel part of the bow shock.

Numerical simulations of this kind of shocks have provided some information about the properties to be expected for the back-streaming protons; they have indeed shown that the shock structure is not stable, but it reforms itself [see *Burgess*, 1989]. The reformation process dominates the shock structure; the cold beams reflected off the shock are found to be rapidly thermalized by this process and may not escape far away from the shock [*Scholer and Burgess*, 1992]. The proton beams far upstream in these simulations are generally found to be hot and almost isotropic.

Dubouloz and Scholer [1993, 1995] modeled the interaction between such a hot beam and the solar wind plasma by injecting, at a given place, a hot ion beam into a cold wind plasma. The beam density is found to globally decay when going against the solar wind. The beam drives RHR modes that scatter the ions and generate regions with high beam ion densities. In these regions the beam distribution is much hotter than in the ambient space and may generate the LHR instability. This mode leads to the growth of left-handed magnetic pulsations that propagate along the magnetic field. They are transported along with the plasma and encounter regions with higher beam densities. These inhomogeneities refract the initially parallel pulsations, which align with the normal to the inhomogeneity and become generally oblique with respect to the ambient magnetic field. The resulting properties of the simulated pulsations are similar to the observed ones.

Another line of thought is to look, as did *Winske and Quest* [1986], whether obliquely propagating waves can play some role in the linear or nonlinear stages. They have compared results of 1-D and two-dimensional (2-D) hybrid simulations for a plasma with a cold beam with high drift velocity and varying relative densities. For low beam densities the most unstable mode was the RHR one, and for higher densities the most unstable case was the LHN one. In both cases they found no important differences between the 2-D and 1-D simulations.

In this paper we revisit the situation analyzed by *Winske and Quest* [1986] to see whether increasing the beam density still further would maintain the basically 1-D character of the beam plasma interaction. We have therefore chosen the following plasma parameters, different from those considered by *Winske and Quest* [1986]: the beam and plasma are assumed to be Maxwellian, the ratios of ambient proton and electron pressure to the magnetic one are $\beta_p = \beta_e = 0.5$, the temperature of the beam is $T_b = T_p$ (T_p is the temperature of ambient protons), the density of the beam is $n_b/n_p = 0.04$ (n_p is the density of the ambient protons), and the velocity of the beam with respect to the ambient electrons is $v_b = 10 v_A$ (v_A is the Alfvén velocity). We suppose a plasma with the ratio of the electron plasma frequency to the electron gyrofrequency $\omega_{pe}/\Omega_e = 200$ (this parameter does not apply for the hybrid code, but we use it for linear theory). Table 1 gives an overview of these parameters for further references.

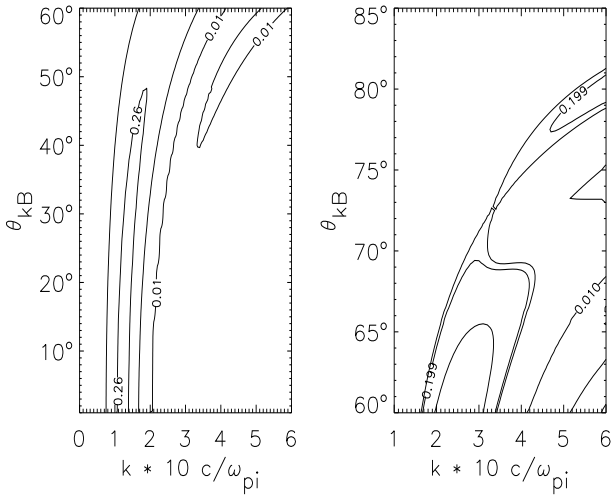

Figure 1. Two-dimensional (2-D) contour plots of the growth rate $\gamma(k, \theta_{\mathbf{kB}})$; for (left) $\theta_{\mathbf{kB}} \leq 60\,\mathrm{deg}$ and (right) $\theta_{\mathbf{kB}} > 60\,\mathrm{deg}$.

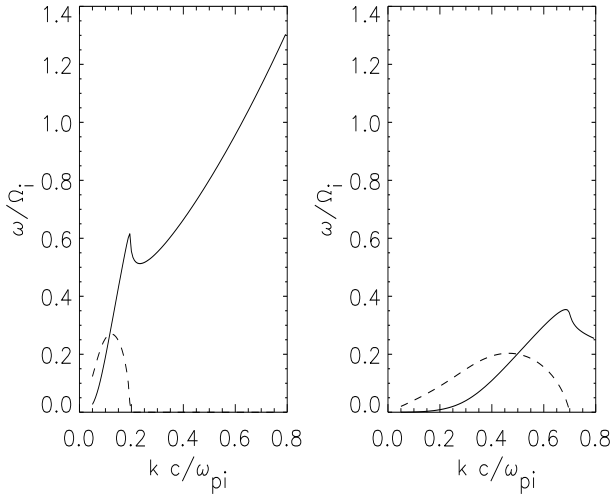

Figure 2. Dispersion relations $\omega(k)$ (solid line) and $\gamma(k)$ (dashed line) for the right-handed resonant (RHR) mode at (left) parallel propagation and (right) oblique propagation of $\theta_{\mathbf{kB}} = 80\,\mathrm{deg}$.

The structure of the paper is the following: first, we study the predictions of linear theory for a beam-plasma system with the parameters given in Table 1. Then, we describe the hybrid code [*Matthews*, 1994] we use to study its nonlinear evolution. After this, we show the results of the simulation, starting with the evolution of global quantities (temperatures and energies); the different stages of the evolution of the system are then analyzed. Finally, we compare the results of the simulation with the prediction of linear theory and with observations. We also compare the results of our simulation with those of the earlier simulation by *Winske and Quest* [1986]. In concluding, we discuss the implication of these results and the problems that remain unresolved.

2. Linear Theory

Linear theory of the electromagnetic ion beam instability is well known [*Gary*, 1991]. Linear theory predicts that the most unstable mode is the electromagnetic RHR mode in parallel propagation. This is illustrated in Figure 1, which displays the results of

a numerical resolution of the dispersion relation, assuming that the beam and the plasma have Maxwellian distribution functions (see *Hellinger and Mangeney* [1997, appendix] for details on the methods used, which are almost identical, in the present case, to those used in the well-known code by *Rönmark* [1982]).

Figure 1 shows 2-D contour plots of the growth rate γ as a function of the magnitude of wave vector $\mathbf{k}$ and of the angle between the $\mathbf{k}$ vector and the ambient magnetic field $\theta_{\mathbf{kB}}$ for $\theta_{\mathbf{kB}} \leq 60\,\mathrm{deg}$ (Figure 1, left) and for strongly oblique propagation, $\theta_{\mathbf{kB}} > 60\,\mathrm{deg}$ (Figure 1, right).

These results are in agreement with the study of *Gary et al.* [1981]; the RHR mode is unstable over a wide range of wave vectors, but, as usual, the most unstable mode is an electromagnetic, circularly polarized wave propagating along the ambient magnetic field, with a wave vector $kc/\omega_{pi} \simeq 0.12$ and a growth rate $\gamma \simeq 0.27\Omega_i$, ($\Omega_i$ is the proton gyrofrequency).

However, our purpose in this section is to show that a qualitatively new feature appears when the relative beam density increases. Note, first, that for the low beam densities that are usually considered, the growth rate of the RHR mode decreases monotonically as the angle $\theta_{\mathbf{kB}}$ of propagation increases [see, e.g., *Gary et al.*, 1981]; this is no longer the case above $n_b/n_p \gtrsim 0.035$ (for the parameters given in Table 1); then the dispersion properties of the beam-plasma system change qualitatively, and we may note the appearance, in Figure 1 (right), of a saddle point at $k_* c/\omega_{pi} \simeq 3.4$ and $\theta_{\mathbf{kB}} \simeq 73\,\mathrm{deg}$ and of a local maximum of the growth rate, $\gamma^o_{\max} \simeq 0.2\Omega_i$, for strongly oblique propagation ($\theta_{\mathbf{kB}} \sim 80\,\mathrm{deg}$), which is almost as high as that of the most unstable parallel propagating wave

The oblique RHR waves are elliptically polarized, have an important electrostatic component $|\mathbf{k}\cdot\delta\mathbf{E}|/|\mathbf{k}\times\delta\mathbf{E}| \sim 10$ and are strongly compressive. Indeed, the compressibility ratio [cf. *Gary*, 1986] of the beam density C_b is very large, $C_b \sim 10$, where C_b is defined as follows:

$$C_b = \frac{\delta n_b B_0}{|\delta\mathbf{B}| n_{b0}} \simeq \frac{\omega\Omega_i}{\omega_{pb}^2}\frac{|\mathbf{k}\cdot\mathbf{D}_b\cdot\delta\mathbf{E}|}{|\mathbf{k}\times\delta\mathbf{E}|}. \quad (1)$$

In these expressions, $\omega_{pb} = (n_b e^2/m_p\epsilon_0)^{1/2}$ is the beam plasma frequency, $\mathbf{D}_b$ is the contribution of the beam to the dispersion matrix $\mathbf{D}$, and the frequency ω and the electric field $\delta\mathbf{E}$ being solutions of the dispersion relation $\mathbf{D}\cdot\delta\mathbf{E} = 0$.

A comparison of the dispersion properties of the most unstable parallel and oblique RHR modes is illustrated in Figure 2, which shows the frequency $\omega(k)$ (solid line) and growth rate $\gamma(k)$ (dashed line) for the RHR mode plotted as functions of wave vector $\mathbf{k}$ for two propagation angles: $\theta_{\mathbf{kB}} = 0\,\mathrm{deg}$ (Figure 2, left) and $\theta_{\mathbf{kB}} = 80\,\mathrm{deg}$ (Figure 2, right). Note, first, that other modes are also destabilized by the beam but they have much smaller growth rates and, second, that similar results were found by *Karimabadi et al.* [1994] in a different context. It is therefore interesting to study numerically the behavior of this beam-plasma system, to see whether the appearance of the compressible, oblique modes has an effect on its nonlinear evolution.

3. Simulations

For the numerical simulation we use the 2-D version of the hybrid code developed by *Matthews* [1994]. In this code the electrons are considered as a massless fluid, with a constant temperature; the ions are treated as particles and are advanced by a leapfrog scheme that requires the fields to be known at half time steps ahead of the particle velocities. This is obtained by advancing the current density to this time step with only one computational pass through the particle data at each time step. Two interlaced grids are used, one with nodes at cell centers for the electric field and the other one with nodes at cell vertices for all the other fields. The particle contribution to the current density at the relevant nodes is evaluated with bilinear weighting followed by smoothing over three points.

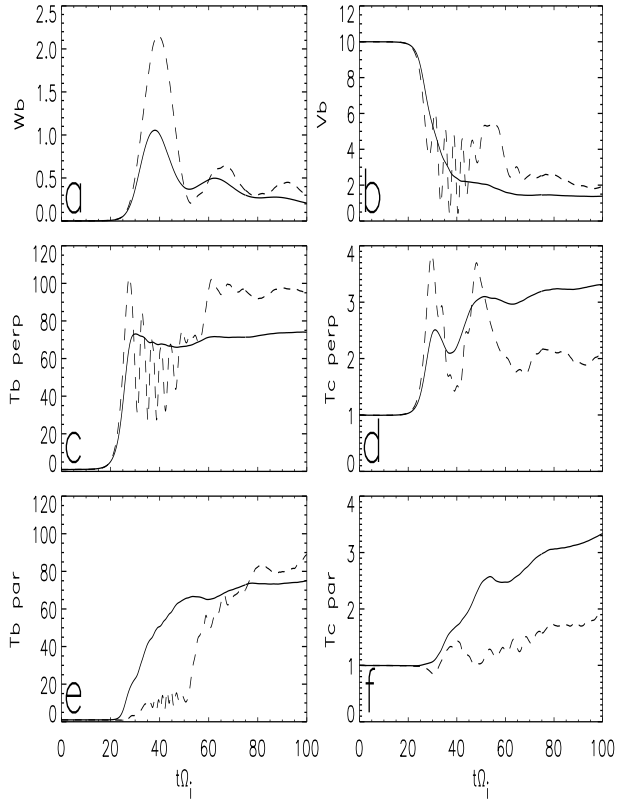

Figure 3. Time histories of the (a) density of the fluctuating magnetic field energy $W_b = (\delta\mathbf{B}/B_0)^2$, (b) beam velocity v_b, and the (c) parallel and (d) perpendicular temperatures of the core plasma and the (e) parallel and (f) perpendicular beam temperatures. The 2-D results denoted by solid lines; 1-D ones are represented by by dashed lines.

No smoothing is performed on the electromagnetic fields, and the resistivity is set to zero in Ohm's law. The magnetic field is advanced in time with a modified midpoint method, which allows time substepping for the advance of the field.

The units and parameters of the simulation are the following: units of space and time are c/ω_{pi} and Ω_i, respectively, where $\omega_{pi} = (n_p e^2/m_p\epsilon_0)^{1/2}$ is the proton plasma frequency and $\Omega_i = eB_0/m_p$ is the proton gyrofrequency. In these expressions, n_p and B_0 are the density of the plasma protons and magnitude of the initial magnetic field, respectively, while e and m_p are the proton electric charge and mass, respectively; and, finally c, ϵ_0, and μ_0 are the speed of light and the dielectric and magnetic permeabilities of vacuum, respectively. The spatial resolution is $dx = dy = c/\omega_{pi}$. There are 60 particles per cell for both the core plasma and the beam protons. The simulation box is in the xy plane and is assumed to be periodic in both dimensions. The fields and moments are defined on a 2-D grid with dimensions $n_x \times n_y = 100 \times 300$. The time step for the particle advance is $dt = 0.01\Omega_i^{-1}$ while the magnetic field $\mathbf{B}$ is advanced with a smaller time step, $dt_B = dt/20$. Velocities are given in units of v_A. The same units are used in all subsequent figures.

We initialize the simulation with a homogeneous proton beam-plasma system in an initially homogeneous magnetic field $\mathbf{B}_0$ directed along the y axis, $\mathbf{B}_0 = (0, B_0, 0)$. The plasma and the beam are Maxwellian, with parameters given in Table 1.

3.1. Evolution of Global Quantities

Let us start the description of the simulation results with the time evolution of the global quantities shown in Figure 3 (solid lines) for the average fluctuating magnetic field energy density

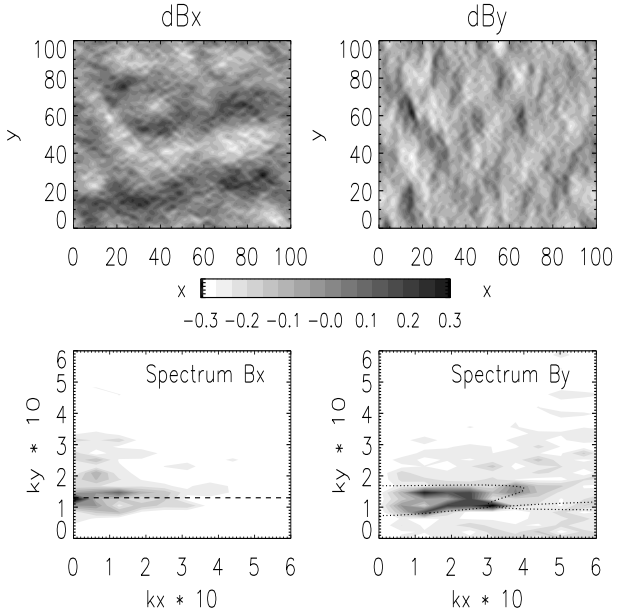

Figure 4. Simulation results at time $t = 20\Omega_i^{-1}$, showing (top) gray level plots (scale shown in middle) of the fluctuating magnetic components (left) δB_x and (right) δB_y. Only one third of the simulation box is shown. (bottom) Gray level plots of corresponding spatial spectra. Black corresponds to the maximum; white corresponds to the minimum. Dashed line (bottom left) indicates the wave vector $\mathbf{k}_y$, where linear theory predicts the maximum growth rate. Dotted line (bottom right) is the $\gamma = 0.195\Omega_i$ contour line replotted from Figure 1.

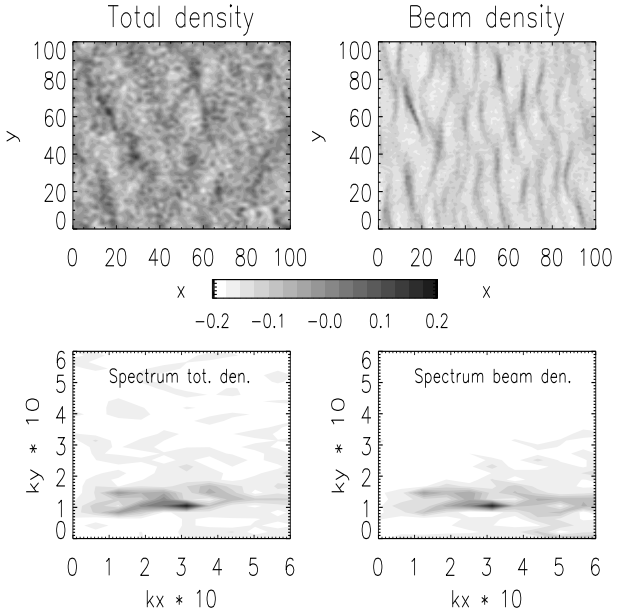

Figure 5. Simulation results at time $t = 20\Omega_i^{-1}$, showing (top) gray level plots (scale shown in the middle) of fluctuating densities for (left) the total δn_t and (right) the beam δn_b. Only one third of the simulation box is shown. of Figure. (bottom) Gray level plots of corresponding spatial spectra. Black corresponds to maximum; white corresponds to minimum.

$W_b = (\delta\mathbf{B}/B_0)^2$ (Figure 3a), the average beam velocity v_b (Figure 3b), and the average parallel (Figure 3c) and perpendicular (Figure 3d) temperatures of the background plasma and beam (Figures 3e and 3f). Temperatures are given in units of their initial value. For comparison we have also plotted the results obtained with a 1-D simulation performed with the same parameters (dashed lines). In both simulations the total energy is well conserved (there is a small gain of energy lower than 1% of the initial total energy).

The evolution of the global quantities in the 1-D and 2-D simulations is similar [cf. *Winske and Quest*, 1986] and is also similar to those observed by *Winske and Leroy* [1984] and *Winske and Quest* [1986] in their respective simulations; there is a phase of exponential growth, around $t = 20\Omega_i^{-1}$, with a growth rate $2\gamma_{\text{eff}} \simeq 0.52\Omega_i^{-1}$, which corresponds to the maximum linear growth rate of the RHR mode in parallel propagation (see Figure 3). This phase is followed by a phase of nonlinear relaxation. However, one may note an important difference between 1-D and 2-D results; early on, $t\Omega_i = 20-30$, the beam protons are heated in the parallel direction in the 2-D simulation, whereas in the 1-D simulation the parallel temperature is about constant (see Figure 3e). This heating is due to the presence of the oblique modes, which turn out to be important for the evolution of the instability, as we see later.

3.2. Linear Stage: Parallel modes

Let us now consider in more detail the results of the first phase of the simulation. During this first stage the magnetic field is dominated by the RHR mode in parallel propagation as shown in Figure 4, top left and top right, which display the gray level plots of the magnetic components of the fluctuation δB_x and δB_y, respectively, at time $t = 20\Omega_i^{-1}$; only one third of the simulation box is shown. The gray scale for these two panels is also displayed, in units of the initial uniform magnetic field. Figure 4, bottom, displays gray level plots of the corresponding spatial spectra $|\tilde{f}(k_x, k_y)|$, where $\tilde{f}(k_x, k_y) = 1/\sqrt{2\pi}\int f(x,y)\exp[i(k_x x + k_y y)]dxdy$. In Figure 4 (bottom) black corresponds to the maximum and white corresponds to the minimum; the limited dynamics does not allow one to follow the fast decrease of the spectra for large wave vectors $k = \sqrt{(}k_x^2 + k_y^2)$, which is somewhat faster than $|\tilde{f}| \propto k^{-5}$, for $kc/\omega_{pi} \geq 1.5$.

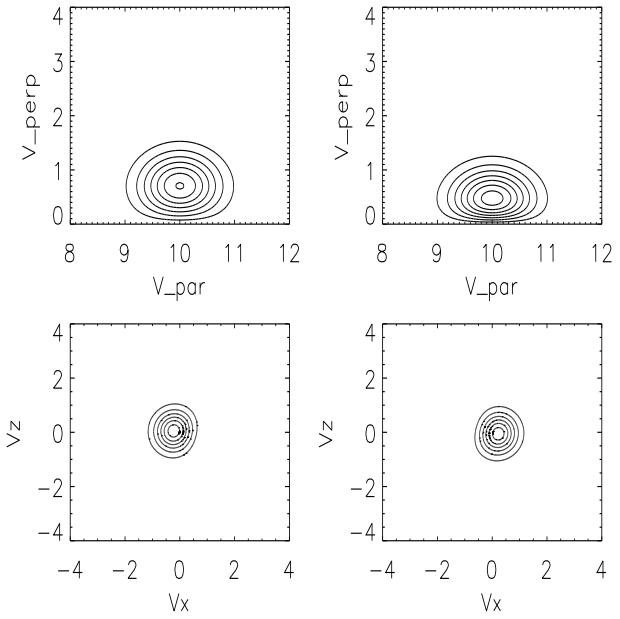

Figure 6. Results from linear theory, showing contours of (top) $v_\perp f_b(v_{||}, v_\perp)$, and (bottom) $f_b(v_x, v_z)$ for (left) maximum and (right) minimum beam density.

Figure 4 shows that during the linear stage a wide range of waves is actually excited, even for highly oblique propagation, as manifested in the spatial variations of δB_y (see Figure 4, right), while

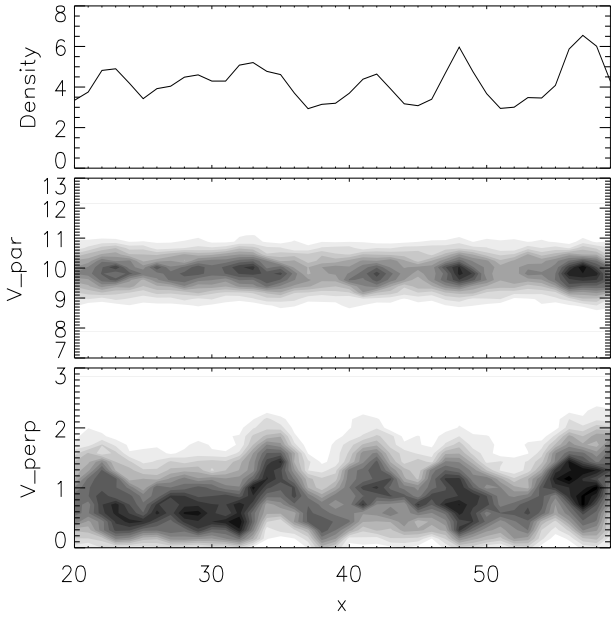

Figure 7. Simulation results at time $t = 18\Omega_i^{-1}$, showing (top) a profile of beam density along the x axis, given in percent of n_p, and gray level plots of (middle) $f_b(x, v_{||})$ and (bottom) $v_\perp f_b(x, v_\perp)$.

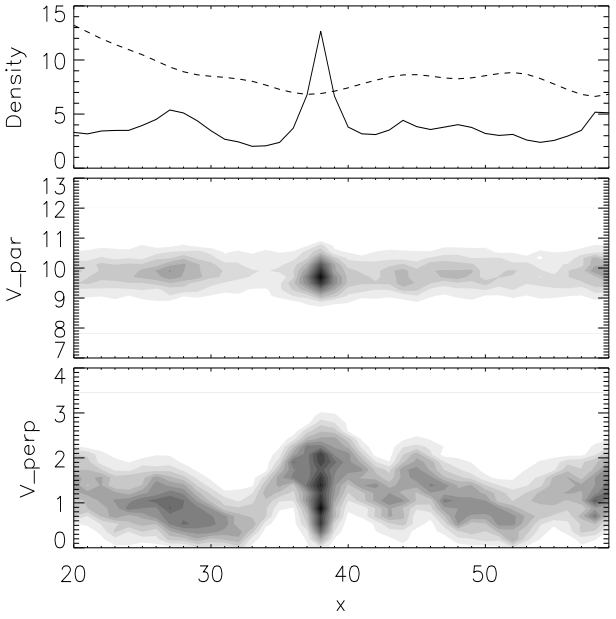

Figure 9. Simulation results at $t = 20\Omega_i^{-1}$, showing (top) a profile of the beam density (in percent of n_p) along the x axis (solid line), with a profile of electric potential V (in arbitrary units) plotted (dashed line) for comparison, and gray level plots of (middle) $f_b(x, v_{||})$ and (bottom) $v_\perp f_b(x, v_\perp)$.

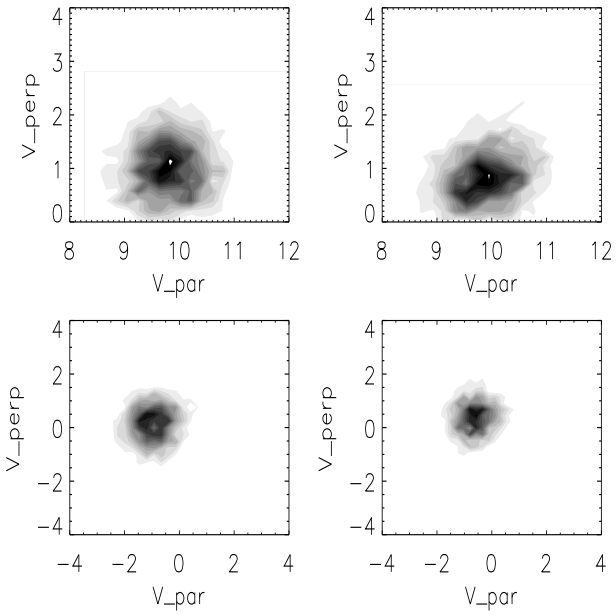

Figure 8. Simulation results at $t = 18\Omega_i^{-1}$, showing gray level plots of (top) $v_\perp f_b(v_{||}, v_\perp)$, and (bottom) $f_b(v_x, v_z)$ for (left) maximum and (right) minimum beam density.

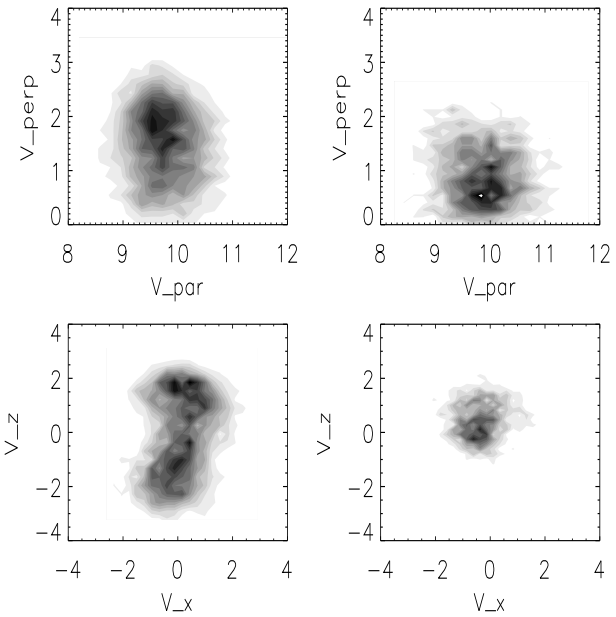

Figure 10. Simulation results at $t = 20\Omega_i^{-1}$, showing gray level plots of (top) $v_\perp f_b(v_{||}, v_\perp)$, and (bottom) $f_b(v_x, v_z)$ for (left) maximum and (right) minimum beam density.

the maximum value of $|\delta\tilde{B}_x(k_x, k_y)|$ occurs for parallel propagation, around the wave vector k_y, where the linear theory predicts the maximum growth rate (indicated by a dashed line). Figure 4 (bottom right) also shows that the amplitude of the oblique modes is highest in the vicinity of the "saddle point" of Figure 1 at $k_* c/\omega_{pi} \simeq 3.4$ and $\theta_{\mathbf{kB}} \simeq 73\,\mathrm{deg}$. For comparison with linear theory, we have replotted (dotted line) the $\gamma = 0.195\Omega_i$ contour line of Figure 1, in order to illustrate the fact that the oblique modes that are present at time $t = 20\Omega_i^{-1}$ belong either to the same branch of the dispersion relation as the parallel mode or to the new branch that appears at high relative beam density.

The fluctuations in the beam density follow rather closely those of δB_y, as seen in Figure 5, which displays, in the same format as Figure 4 (and at the same time $t = 20\Omega_i^{-1}$), the spatial variations of the fluctuating total δn_t and beam δn_b densities together with their Fourier spectrum. As expected from linear theory, the oblique modes are compressive, as can be seen throughout Figure 5.

However, the density fluctuations have already reached a nonlinear stage; this is apparent in Figure 5, top right, where one can observe long and narrow regions with large fluctuations in the beam

density, typically of the order of the average beam density itself, $\delta n_b \sim n_b$. For convenience, these structures are called "filaments" in what follows. They have a typical width approximately a few c/ω_{pi}, and a typical length $\sim 10 - 20 c/\omega_{pi}$ and are almost aligned with the ambient magnetic field. A typical distance between two filaments is $\sim 10 c/\omega_{pi}$.

3.3. Wave-Particle Interactions: Linear Stage

To understand why the growth of the unstable oblique modes may lead to the filamentation of the beam, it is interesting to study the interaction of the beam particles with these waves when they are still in the linear stage of their evolution. Note, first, that beam particles may be in resonance $k_{||} v_{||} + l\Omega - \omega \simeq 0$ with the oblique waves as well as with the parallel ones. Let us calculate, then, the perturbed beam distribution function that would be obtained, within the framework of linear theory, if only one unstable oblique wave with $k = 0.46 c/\omega_{pi}$ and $\theta_{\mathbf{kB}} = 80\,\mathrm{deg}$ (see Figure 2) is present. For that we use the expression

$$\delta f_b(v_{||}, v_\perp, \phi) = \mathrm{Re}\left(\frac{iq}{m} e^{i\lambda \sin\phi} \sum_{l=-\infty}^{\infty} \frac{\mathbf{a}_l \cdot \delta\mathbf{E} e^{-il\phi}}{k_{||} v_{||} + l\Omega - \omega} \right) \quad (2)$$

which is given by *Pantellini et al.* [1994] or *Woodcock* [1995]. The electric field perturbation is taken in the form of a plane wave $\delta\mathbf{E} \propto \exp[i(\mathbf{k}\cdot\mathbf{x} - \omega t)]$, and we have used the definitions $\lambda = k_\perp v_\perp/\Omega$, $v_x = v_\perp \cos\phi$, and $v_z = v_\perp \sin\phi$, while $\mathbf{a}_l$ depends on $v_{||}$, $v_\perp$, $\mathbf{k}$, and ω as well as on the unperturbed distribution functions of the beam f_{0b} and background plasma f_{0p}; a detailed expression is given by *Woodcock* [1995]. Figure 6 displays some properties of the total beam distribution function $f_b = f_{0b} + \delta f_b$, calculated in this way, near a maximum (Figure 6, left) and minimum (Figure 6, right) of the beam density. Figure 6 (top) shows contours of the "weighted" distribution function $v_\perp f_b(v_{||}, v_\perp)$, while Figure 6 (bottom) shows contours of the distribution $f_b(v_x, v_z)$ of velocities in a plane perpendicular to the unperturbed magnetic field. One may notice a significant difference in the beam distributions between the beam density maxima and minima; there are more particles with high perpendicular speed near a maximum than near a minimum, and the density modulation appears to be due almost entirely to those particles, which happen to be in resonance ($k_{||} v_{||} - \omega \simeq +\Omega_i$) with the wave. On the other hand, Figure 6 (bottom) shows that the contour levels of $f_b(v_x, v_z)$ have lost their circular symmetry around the unperturbed magnetic field, which is evidence that the beam particles are bunched in gyrophase by the wave.

To compare these predictions of linear theory with the results of the simulation in its early stages ($t = 18\Omega_i^{-1}$), we present in Figure 7 the phase space of the beam protons at time $t = 18\Omega_i^{-1}$ in a small region of size $40 c/\omega_{pi} \times 10 c/\omega_{pi}$ of the simulation box. Figure 7 (top) shows a profile of the beam density along the x axis, averaged over the y direction, and given in percent of the initial background plasma proton density n_p. Figure 7, middle and bottom, show the gray level plots of the reduced distribution functions $f_b(x, v_{||})$ and $v_\perp f_b(x, v_\perp)$, respectively, also integrated in y. The distribution function $f_b(x, v_{||})$ in parallel velocities (Figure 7, middle) is apparently affected only through the density, $f_b(x, v_{||}) \sim n_b(x) \exp[-(v_{||} - v_b)^2/v_{thb}^2]$, while the distribution function $v_\perp f_b(x, v_\perp)$ in perpendicular velocities has lost its initial Maxwellian shape since, in the vicinity of beam density maxima, the most probable perpendicular speed is significantly higher than the Maxwellian value. More precisely, Figure 8 shows, in gray scale plots with the same format as Figure 6, the beam distribution functions obtained in the region shown in Figure 7 both near a maximum ($40 \le x\omega_{pi}/c \le 43$) and a minimum ($43 \le x\omega_{pi}/c \le 47$) of the beam density. The simulation and linear theory display the same differences between the distribution functions $v_\perp f_b(v_{||}, v_\perp)$ calculated near the maximum and near the minimum of the beam density, with an excess of particles of high perpendicular speed near the maximum. Figure 8 (bottom) indicates as well that the dominant oblique mode has broken the gyrotropic invariance of the beam protons. Thus, at least at the qualitative level, there is a very good agreement between the simulation results and linear theory. A more quantitative comparison of the particle properties of linear theory and the simulation would be difficult, because a wide spectrum of waves of different properties is present in the simulation. In particular, we have to note that linear theory predicts a perpendicular beam temperature lower than that measured in the simulation, which is probably due to the presence of the nearly parallel modes, which increase the perpendicular temperature [cf. *Winske and Quest*, 1986].

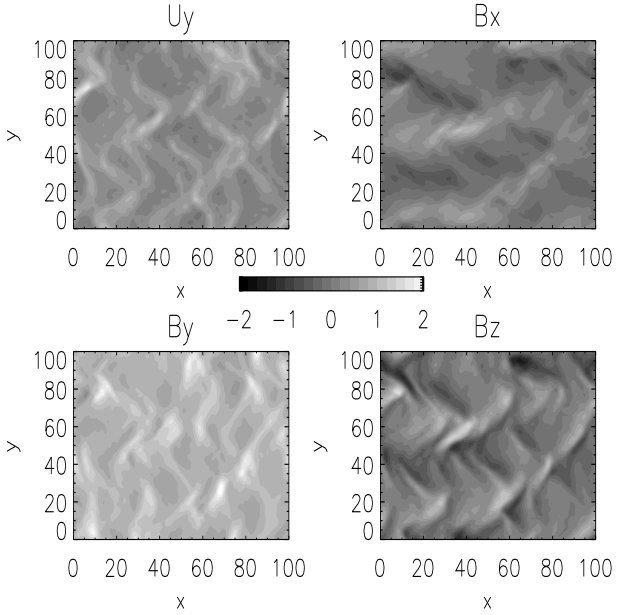

Figure 11. Simulation results at time $t = 30\Omega_i^{-1}$, showing gray level plots of (top left) mean velocity U_y and components (top right) B_x, (bottom left) B_y, and (bottom right) B_z. The gray scale used is displayed in the middle.

We can now understand why the oblique modes (and the associated density fluctuations) reach the nonlinear stage so rapidly, at times when the most unstable parallel modes are still in the linear stage. The parallel modes are essentially electromagnetic, so that any particle trapping will have only a limited effect on the density. On the other hand, the oblique modes are quasi-electrostatic, and particle trapping will have a substantial effect on the beam density with profound consequences on the development of the instability.

3.4. Evolution of Oblique Modes: Filaments

Let us now discuss the nonlinear phase of the oblique modes. Figure 9, which has the same format as Figure 7, shows what happens $2\Omega_i$ later, i.e., at time $t = 20\Omega_i$, to the particles which were at time $t = 18\Omega_i^{-1}$ in the region displayed in Figure 7; in order to follow these particles, we have selected, for display, a region of the simulation box that has been shifted by $\Delta y = 2\Omega_i^{-1} v_b = 20 c/\omega_{pi}$ with respect to that corresponding to Figure 7. Note that the dashed line in the Figure 9 (top) is the profile of the electrostatic potential $V = -\int E_x dx$ (given in arbitrary units). One can observe that a very large peak in the beam density $n_b/n_p \sim 10\%$ has developed in the vicinity of a minimum of the potential V; this is not an exceptional event but represents a typical case of the nonlinear stage of the oblique, compressive mode.

As in the linear phase, the distribution function $f_b(x, v_{||})$ in parallel velocities depends on space only through the density, while the distribution function $v_\perp f_b(x, v_\perp)$ is severely distorted near the density maximum. This appears more clearly in Figure 10, which displays, in the same format as Figure 8, the distributions

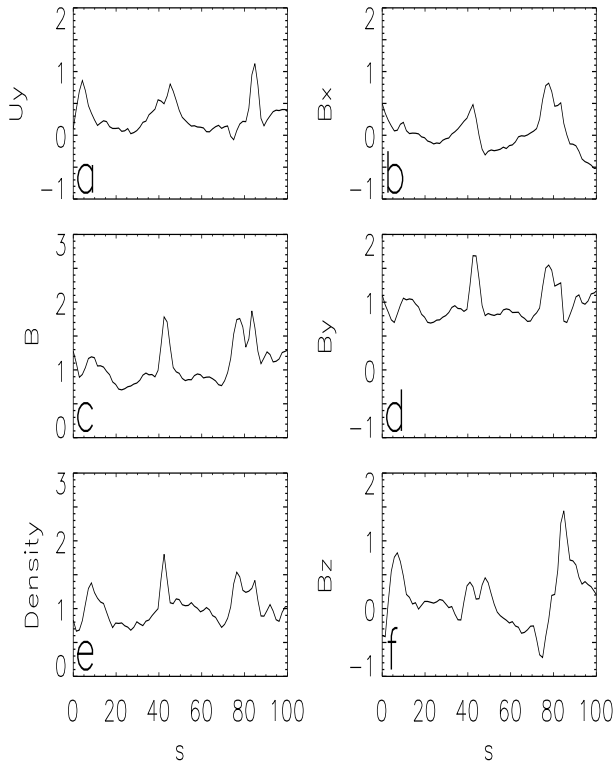

Figure 12. Profiles along the diagonal line s of Figure 11 of (a) U_y, (b) B_x, (c) B, (d) B_y, (e) total density, and (f) B_z.

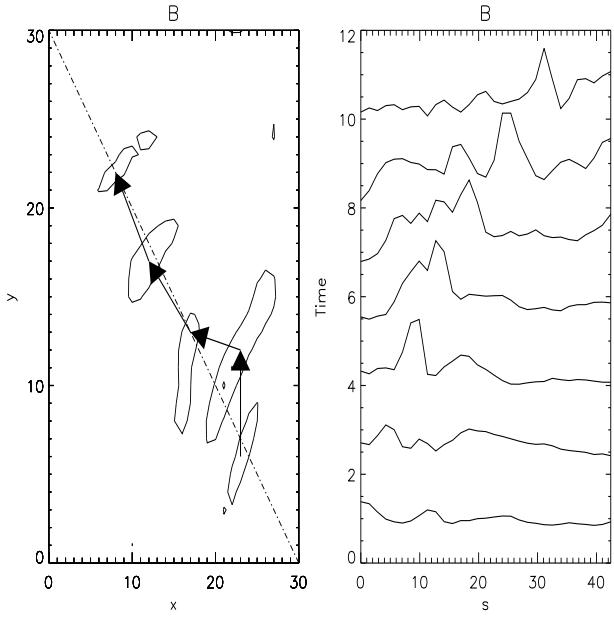

Figure 13. (left) Contours $B = 2.4B_0$ at five different times. Arrows show the time direction and connect the places with the maximum value of B at these times (only part of the simulation box is shown; the dot-dashed line displays the approximate direction of propagation and the place where the profiles of Figure 13, right panel is taken). (right) Spatial profiles of B (at an oblique direction denoted by solid line in Figure 13 left) stacked in time (the time difference between two successive stacked profiles is $2/\Omega_i$). Time is given in arbitrary units.

either in the vicinity of the local maximum of the beam density ($x \sim 36 - 40c/\omega_{pi}$, see Figure 9) or in the vicinity of the minimum of the beam density ($x \sim 31 - 36c/\omega_{pi}$). One may see that near the peak density, most of the beam particles have high perpendicular velocities; they interact strongly with the oblique mode of linear theory (see Figure 6). They are strongly gyrophase bunched, in agreement with linear theory (Figure 10, bottom left, and Figure 6, right). Note that the particles near the minimum of density are strongly gyrophase bunched as well.

The peak in beam density seen in Figure 9 is actually a cross section of one of the filaments seen in Figure 5, corresponding to large fluctuations in the beam density $\delta n_b/n_b \sim 1$. The properties of the filaments are therefore consistent with the supposition that they are formed in the nonlinear stage of the oblique RHR modes by trapping of beam protons in resonance with the waves.

The waves have a lower phase velocity than the resonant beam particles, a fact permitted in cyclotron resonance; therefore these particles that are bunched into filaments of finite length and cross section remain in resonance only for a limited time. This leads to the saturation of the instability, an unusual mechanism based on a sort of space-localized trapping. These are typically 2-D effects. Indeed, we performed 1-D simulations of the nonlinear evolution of the oblique mode with the same parameters as those used; the saturation level is much stronger with stronger density fluctuations since the concentrations in resonant particles are then of infinite extent in the direction perpendicular to the wave propagation.

3.5. Evolution of Beam Filaments

We now consider the evolution of the beam filaments. They are initially almost aligned with the ambient magnetic field; but as time goes on, the filaments interact with the growing parallel modes and become curved. The reason for this effect is simple: the parallel modes make the magnetic field lines oscillate, and the filament protons are forced to follow them. The filaments generate oblique structures in the magnetic field, which appear very clearly in Figure 11, which shows gray level plots of the y component of the bulk velocity U_y (proportional to the beam density) and of the components B_x, B_y, and B_z of the magnetic field, at time $t = 30\Omega_i^{-1}$ in part of the numerical box (the gray scale used is displayed in Figure 11, middle).

Figure 12 shows profiles of variations of the same quantities (plus the total density) along line s of Figure 11, joining the points $(0, 100)c/\omega_{pi}$ and $(29.3, 70.7)c/\omega_{pi}$. The direction along s is, as we see later, an approximate direction of propagation of the magnetic structures. Figures 11 and 12 show strong evidence that magnetic structures are correlated with the regions of high beam (or total) density.

While the "parallel" magnetic energy $E_{B||} \propto \int B_y^2 dxdy$ remains almost constant throughout the simulation, we observe the development of regions of high amplitudes of δB_y, $\delta B_y \sim B_0$, in the vicinity of the regions of the high beam density. A natural explanation is that the magnetic field is swept up by the filaments, during their motion, which is strongly oblique with respect to the main component of the magnetic field. In these regions of high $\delta B_y \sim B_0$ we find also peaks of the total plasma density and the "perpendicular" magnetic energy $E_{B\perp} \propto \int (B_x^2 + B_z^2) dxdy$ indicating that the core plasma and the perpendicular magnetic field are also swept up by the filaments. Note that *Thomas and Brecht* [1988] observed similar effects in 2-D hybrid simulations. They have shown that a strong, finite-sized proton beam is able to push the plasma and magnetic field out of a certain region, forming a diamagnetic cavity.

Let us call these structures of large magnetic field fluctuations $\delta B/B_0 \sim 2$ "pulses." They propagate obliquely $\sim 45^\circ$ with respect to the ambient magnetic field with velocities $\sim 2 - 6v_A$, as shown in Figure 13 (left), displaying the time evolution in the xy plane of the isocontour $B = 2.4B_0$ of a typical pulse. The arrows show the time direction and connect the successive locations of the maximum value of B; the dot-dashed line is the approximate direction of propagation of the pulse and is line s of Figure 11 (note that only part of the simulation box is shown). Figure 13 (right) shows the spatial profiles of B along line s stacked in time (the time difference between two successive stacked profiles is $2/\Omega_i$), with the

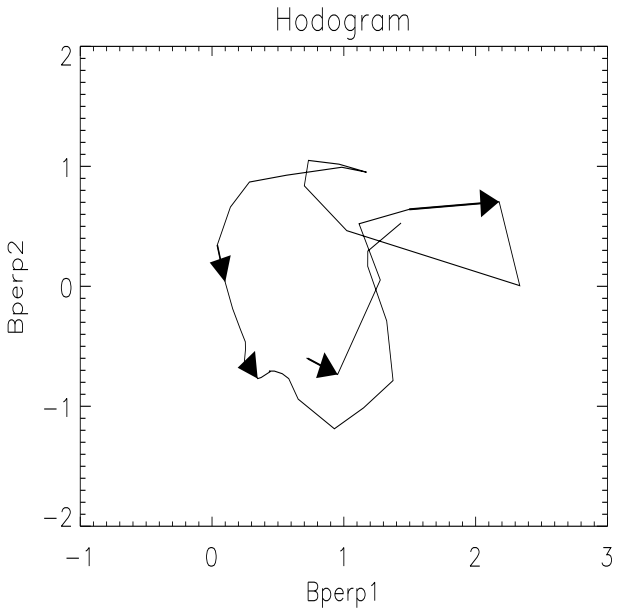

Figure 14. Hodogram of the components of the magnetic field perpendicular to the approximative direction of the propagation.

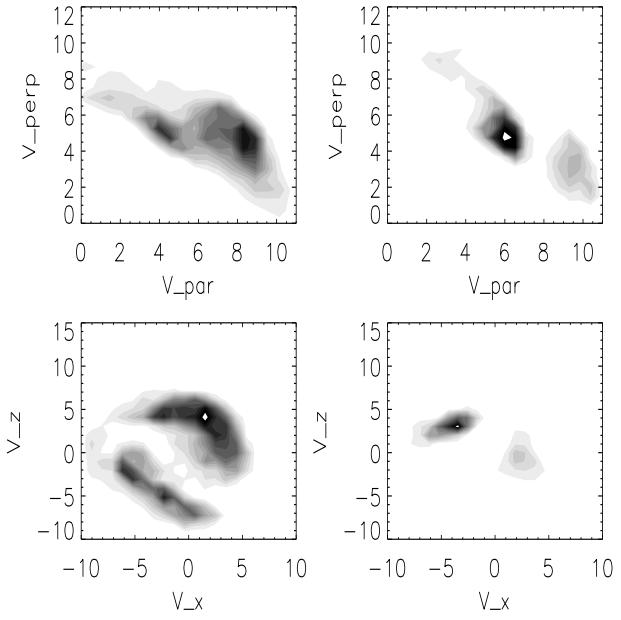

Figure 15. Simulation results at $t = 30\Omega_i^{-1}$, showing (top) gray level plots of the reduced distribution functions $v_\perp f_b(v_{||}, v_\perp)$ of the beam (left) near the pulse and (right) far from it. (bottom) Gray level plots of corresponding $f_b(v_x, v_z)$ (left) near the pulse and (right) the far from it.

magnetic field amplitude given in arbitrary units, illustrating the propagation of the pulse along s at velocity $2 - 6v_A$, increasing with the amplitude of the pulse.

To determine the polarization of the pulses, we have plotted the hodograms of the components of magnetic field perpendicular to the approximative direction of the propagation (like line s of Figure 13, left) and taken along this direction through a pulse. The result of this analysis is that the pulses are generally left-handed in the plasma frame, with a complicated polarization structure. Figure 14 shows an example of such a hodogram for the pulse illustrated in Figure 13. One may see that the polarization is rather complex:

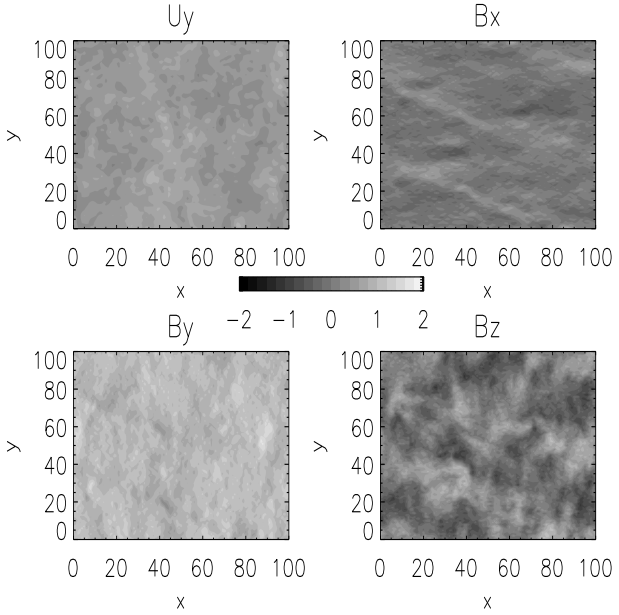

Figure 16. Simulation results at $t = 100\Omega_i^{-1}$, showing gray level plots of (top left) mean velocity U_y and components (top right) B_x, (bottom left) B_y and (bottom right) B_z. The gray scale used is displayed in the middle.

an elliptically polarized right-handed wave with $\delta B_\perp / B_0 \sim 1/2$ surrounds the left-handed, highly elliptically polarized, nonlinear pulse with $\delta B_\perp / B_0 \sim 1$.

A possible explanation of the observed left-hand polarization of the pulses may be found in the severe deformation of the distribution of the beam protons. This is, indeed, the case of the distribution function of protons, which are displayed in Figure 15 in the vicinity of a pulse (left panels) and in a more "quiet region" outside of pulses (right panels). Figure 15 (top) shows the distribution function $f_b(v_{||}, v_\perp)$, while Figure 15 (bottom) displays the distribution $f_b(v_x, v_z)$, with parallel and perpendicular velocities being defined with respect to the unperturbed magnetic field $\mathbf{B}_0$. We can see that the beam has slowed down and that the beam distribution function is strongly gyrophase bunched; the beam distribution may be partly described as a ring-beam distribution.

For such beam distributions (which are strongly anisotropic, and even ring-like) the left-handed resonant mode in oblique propagation may become important at sufficient high beam density [see *Gary et al.*, 1984; *Smith and Gary*, 1987; *Karimabadi et al.*, 1994]. So the left-handed polarization of the pulses may be explained by the resultant amplification of the left-handed resonant mode; this could explain both the pulse growth observed in Figure 13 and the change from the highly oblique propagation, characteristics of the quasi-electrostatic mode, to the less oblique propagation of the pulses in the LHR mode [*Gary et al.*, 1984; *Smith and Gary*, 1987]. The excitation of the LHR mode might thus be the resonant mechanism that we have invoked for the generation of the strong fluctuation of B_z and B_x. It remains to be shown that with the observed beam distributions the relevant instability has enough time to develop, an effort which is left for future work.

3.6. Final State

The plasma-beam system ends up in a highly turbulent medium. This is shown in Figure 16, which displays, in the same format as Figure 11, the results of the simulation at time $t \sim 100\Omega_i^{-1}$, in a limited portion (one third) of the simulation box. It is hard to see any structure; besides, the parallel and perpendicular temperatures of both the core and beam protons are then almost equal. A careful analysis shows that, in this stage of the simulation, the beam particles get reflected on the oblique pulses and are rapidly thermalized.

4. Comparison With Foreshock Pulsations

We have shown that oblique modes with growth rates lower than, but comparable to, those of the parallel modes may significantly influence the nonlinear behavior of the plasma-beam system, above a certain relative beam density. These oblique modes are highly compressive and lead nonlinearly to a filamentation of the beam, with large fluctuations in the beam density ending up in the formation of finite-length filaments that interact strongly with the plasma.

The beam filaments sweep up the magnetic field and the core plasma and generate through a resonant mechanism magnetic pulses of high amplitudes $\delta B/B_0 \sim 2$. These pulses, which have typical widths $\sim 5 - 10 c/\omega_{pi}$ and typical lengths $\sim 10 - 20 c/\omega_{pi}$, propagate obliquely with respect to the ambient magnetic field with a velocity of the order of $\sim 2 - 6 v_A$, increasing with the amplitude of the pulse. The pulses themselves are left-handed in the plasma frame but are usually surrounded by right-handed waves.

It is worthwhile to compare these results with the observations of magnetic pulses in the quasi-parallel terrestrial foreshock [*Thomsen et al.*, 1990; *Schwartz et al.*, 1992; *Mann et al.*, 1994]. They have indeed a number of properties in common. As the pulses observed in the simulations, those observed in the foreshock are found to propagate against the solar wind obliquely with respect to the ambient magnetic field. They are left-handed in the plasma frame, and their velocity is $\sim 2 - 4 v_A$, increasing generally with the amplitude. Their scale lengths are generally smaller than the wavelength of ULF waves and comparable to those of the simulation pulses.

In the simulation we observe a significant correlation between the magnitude of the magnetic field and the density, which is not so apparent in the observations [*Thomsen et al.*, 1990; *Schwartz et al.*, 1992]; but the most significant difference concerns the amplitudes. In the foreshock they often reach large amplitudes $\delta B/B_0 \sim 3 - 5$, significantly larger than those obtained in the simulations. This may be perhaps explained by the fact that in the foreshock there is a more or less stable influx of beam particles, allowing the pulses to reach higher amplitudes than in the present simulations, where the beam relaxes to a state where its free energy has disappeared.

Two other points are worth mentioning. First, a recent work by *Giacalone et al.* [1993] has shown that the SLAMS are generally associated with strong gradients of suprathermal particle density, which appear near the trailing edge of the SLAMS. *Giacalone et al.* [1993] suggest that these gradients are due to the fact that the SLAMS "sweep up" the ions as they move through the plasma. This process is similar to what we observe in our simulations, where the thermal plasma particles are also swept up by the propagating pulses while being only slightly adiabatically heated. Assuming that the physical processes are basically the same in the simulations and in the foreshock, all particles, both thermal and suprathermal, would be swept up as well, but the effect would be more apparent for the suprathermal particles.

Second, observations of the proton foreshock by *Wilkinson et al.* [1993] show strong protons beams (up to about 10% of ambient plasma density) that are localized in narrow space regions. These beams are somewhat reminiscent of the filaments observed in the simulation, but the wave activity found by *Wilkinson et al.* [1993], along with these beams, is low and does not easily compare to the results of the simulation.

To conclude this comparison with observations, let us stress that the results of the simulation suggest that kinetic effects of the beam protons are important for the generation of SLAMS. Therefore a detailed study of the distribution functions within and near SLAMS is evidently needed to be able to make a more quantitative comparison. Such a study is not presently available.

5. Discussion

As already mentioned several times, the results of 1-D simulations are qualitatively different [see also *Onsager et al.*, 1991; *Akimoto et al.*, 1993]; in particular, the pulses observed by *Akimoto et al.* [1993] have different properties from those described above. It is therefore important to check that 2-D simulations are representative of the physics under consideration. We have performed three-dimensional (3-D) simulations but in a smaller numerical domain (100^3, $dx = dy = dz = 2c/\omega_{pi}$), and we have observed qualitatively similar phenomena, the formation of filaments of similar sizes and amplitudes, with a spiral shape and an elliptical cross section. In the late stages of the simulation we observed also the appearance of localized 3-D magnetic pulsations with characteristic sizes and properties similar to those found in the 2-D simulations. Note that *Thomas* [1989] observed similar effects in 3-D hybrid simulations, which were an extension of the previous 2-D simulations of diamagnetic cavities by *Thomas and Brecht* [1988].

One may wonder why such structures have not been observed in previous two-dimensional simulations of the electromagnetic ion beam instabilities. *Winske and Quest* [1986] have done two simulations for two special cases, low- and high-density beam. In both cases some oblique modes are present during the linear stage but the parallel modes dominate the simulation in the nonlinear stage. In the case of the high density beam the simulation of *Winske and Quest* [1986] was dominated by the nonresonant parallel mode, so the simulation is not comparable to ours. However, in the case of low-density beam (1.5% of the total plasma density) the physical situation is similar to ours; the parallel resonant mode has the maximum growth rate, but oblique modes are also unstable with a lower growth rate. It is difficult to assert the precise reasons why, in our simulations, the nonlinear evolution is so different from the results of *Winske and Quest* [1986]. One possibility could be that the spatial resolution of the simulation by *Winske and Quest* [1986] is only $2c/\omega_{pi}$, so that the oblique modes with wavelengths ~ 10 are not well resolved, an effect that is strengthened by the three-point smoothing 1/4-1/2-1/4 of the electric field, which must numerically damp these nearly electrostatic waves. Another, more subtle reason may be related to the fact that linear theory predicts that the growth rate of the oblique modes decreases when the beam temperature increases and/or when the beam velocity decreases. Thus, if for some reason there is an important heating or slowing down of the beam due, for example, to the quasi-linear relaxation, oblique modes may be suppressed. Moreover, the ratio $\gamma_o/\gamma_{||}$ (where γ_o is the growth rate of the oblique mode and $\gamma_{||}$ is the growth rate of the parallel mode) decreases when the beam density decreases.

A third explanation may be that the results of the simulation depend on the initial noise introduced in the simulation; the rms electric amplitudes of the compressible modes with oblique wave vectors should be comparable to those of the electromagnetic modes with parallel wave vectors, if one wants to study the effects of these oblique modes. If the parallel modes have a much larger initial level, they will dominate the simulation at any time.

To conclude this discussion, we may speculate about the effects of finite mass electrons. The beam compression and filamentation are due to low frequency, almost electrostatic waves that trap resonant beam protons. The electrons react to the potential so as to smooth it and limit the trapping of beam protons; taking into account their inertia, they will reduce only very slightly this effect. Therefore we do not expect a significant influence of electrons on beam filamentation; however, such speculation should be tested.

6. Conclusion

We have shown that for relatively dense proton beams the oblique modes may play an important role in the nonlinear stage of the electromagnetic instability, even when the linearly dominant modes are the parallel ones. A very important aspect is the fact that the beam particles are resonant both with the oblique and parallel modes. However, trapping in the parallel mode does not produce density fluctuations at lowest order (however, at higher orders it does; see *Akimoto et al.* [1991, 1993]), but trapping in the compressible oblique modes produces first-order density fluctuations. Thus the trapped protons become localized in space, and the beam takes a filamentary structure; the beam filaments interact with the nearly parallel waves generated by the ambient beam protons, an

interaction which curves the filaments. During this period the filaments sweep the magnetic field and cause the appearance of regions of large amplitudes of δB_y. The core plasma is partially swept along, and a large density fluctuation appears. The beam distribution functions become highly anisotropic and may amplify the magnetic fluctuations, which, created in this way, are forming magnetic pulses with left-hand polarization and propagation directions intermediate between that of the initially unstable oblique modes and the unperturbed magnetic field.

We expect that similar nonlinear behavior of the beam-plasma system may arise when the oblique modes have a growth rate comparable to the most unstable parallel modes and when the initial level of fluctuation of these modes is of the same order. These oblique modes may be important for the structure and dissipation within the Earth's bow shock; but more realistic simulations and more detailed comparisons with observations are needed to determine the role of these oblique modes. This will be the subject of future work.

Acknowledgments. Michel Blanc thanks two referees for their assistance in evaluating this paper.

References

Akimoto, K., D. Winske, T. G. Onsager, M. F. Thomsen, and S. P. Gary, Steepening of parallel propagating hydrodynamic waves into magnetic pulsation: a simulation study, *J. Geophys. Res.*, *96*, 17,599–17,607, 1991.

Akimoto, K., D. Winske, S. P. Gary, and M. F. Thomsen, Nonlinear evolution of electromagnetic ion beam instabilities, *J. Geophys. Res.*, *98*, 1419–1433, 1993.

Burgess, D., Cyclic behavior at quasi-parallel collisionless shocks, *Geophys. Res. Lett.*, *16*, 345–349, 1989.

Dubouloz, N., and M. Scholer, On the origin of short large-amplitude magnetic structures upstream of quasi-parallel collisionless shocks, *Geophys. Res. Lett.*, *20*, 547–550, 1993.

Dubouloz, N., and M. Scholer, Two-dimensional simulations of magnetic pulsation upstream of the Earth's bow shock, *J. Geophys. Res.*, *100*, 9461–9474, 1995.

Elaoufir, J., A. Mangeney, T. Passot, C. C. Harvey, and C. T. Russell, Large amplitude MHD waves in the Earth's proton foreshock, *Ann. Geophys.*, *8*, 297–314, 1990.

Fuselier, S. A., M. F. Thomsen, F. M. Ipavich, and W. K. H. Schmidt, Suprathermal He^{2+} in the Earth's foreshock region, *J. Geophys. Res.*, *100*, 17,107–17,116, 1995.

Gary, S. P., Low-frequency waves in a high-beta collisionless plasma: Polarization, compressibility and helicity, *J. Plasma Phys.*, *35*, 431–447, 1986.

Gary, S. P., Electromagnetic ion/ion instabilities and their consequences in space plasma: A review, *Space Sci. Rev.*, *56*, 373–414, 1991.

Gary, S. P., J. T. Gosling, and D. W. Forslund, The electromagnetic ion beam instability upstream of the Earth's bow shock, *J. Geophys. Res.*, *86*, 6691, 1981.

Gary, S. P., C. W. Smith, M. A. Lee, M. L. Goldstein, and D. W. Forslund, Electromagnetic ion beam instabilities, *Phys. Fluids*, *27*, 1852–1862, 1984.

Giacalone, J., S. J. Schwartz, and D. Burgess, Observation of suprathermal ions in association with the SLAMS, *Geophys. Res. Lett.*, *20*, 149–152, 1993.

Hada, T., C. F. Kennel, and T. Teresawa, Excitation of compressional waves and the formation of shocklets in the Earth's foreshock, *J. Geophys. Res.*, *99*, 21,541–21,556, 1987.

Hellinger, P., and A. Mangeney, Upstream whistlers generated by protons reflected from a quasi-perpendicular shock, *J. Geophys. Res.*, *102*, 9809–9819, 1997.

Ipavich, F. M., G. Gloekler, D. C. Hamilton, L. M. Kistler, and J. T. Gosling, Protons and alpha particles in field aligned beams upstream of the bow shock, *Geophys. Res. Lett.*, *15*, 1153–1156, 1988.

Karimabadi, H., D. Krauss-Varban, N. Omidi, S. A. Fuselier, and M. Neugebauer, Low frequency instabilities and the resulting velocity distributions of pick-up ions at comet Halley, *J. Geophys. Res.*, *92*, 4423–4435, 1994.

Mann, G., H. Lühr, and W. Baumjohann, Statistical analysis of short large-amplitude magnetic field structures in the vicinity of the quasi-parallel bow shock, *J. Geophys. Res.*, *99*, 13,315–13,323, 1994.

Matthews, A., Current advance method and cyclic leapfrog for 2D multispecies hybrid plasma simulations, *J. Comput. Phys.*, *112*, 102–116, 1994.

Omidi, N., and D. Winske, Steepening of kinetic magnetosonic waves into shocklets: simulations and consequences for planetary shocks and comets, *J. Geophys. Res.*, *95*, 2281–2230, 1990.

Onsager, T. G., D. Winske, and M. F. Thomsen, Interaction of a finite-length ion beam with a background plasma: reflected ions at the quasi-parallel bow shock, *J. Geophys. Res.*, *96*, 1775–1788, 1991.

Pantellini, F. G. E., D. Burgess, and S. J. Schwartz, Phase space evolution in linear instabilities, *Phys. Plasmas*, *1*, 3784, 1994.

Rönmark, K., WHAMP-waves in homogeneous, anisotropic, multicomponent plasmas, *Tech. Rep. 179*, Kiruna Geophysical Institute, 1982.

Scholer, M., Upstream waves, shocklets, short large-amplitude magnetic structures and the cyclic behavior of oblique quasi-parallel collisionless shocks, *J. Geophys. Res.*, *98*, 47–57, 1993.

Scholer, M., and D. Burgess, The role of upstream waves in supercritical quasi-parallel shock re-formation, *J. Geophys. Res.*, *97*, 8319–8326, 1992.

Schwartz, S. J., D. Burgess, W. P. Wilkinson, R. L. Kessel, M. Dunlop, and H. Lühr, Observation of short large-amplitude magnetic structures at a quasi-parallel shock, *J. Geophys. Res.*, *97*, 4209–4227, 1992.

Smith, C. W., and S. P. Gary, Electromagnetic ion beam instabilities: growth at cyclotron harmonics, *J. Geophys. Res.*, *92*, 117, 1987.

Thomas, V. A., Three-dimensional simulation of diamagnetic cavity formation by a finite-sized plasma beam, *J. Geophys. Res.*, *94*, 13,579–13,583, 1989.

Thomas, V. A., and S. H. Brecht, Evolution of diamagnetic cavities in the solar wind, *J. Geophys. Res.*, *93*, 11,341–11,353, 1988.

Thomsen, M. F., J. T. Gosling, S. J. Bame, and C. T. Russell, Magnetic pulsations at the quasi-parallel shock, *J. Geophys. Res.*, *95*, 957–966, 1990.

Tsurutani, B. T., and R. G. Stone (Eds.), *Collisionless shocks in the Heliosphere: Review of Current Research*, *Geophys. Monograph. Ser.*, vol. 35, AGU, Washington, D. C., 1985.

Wilkinson, W. P., A. K. Pardaens, S. J. Schwartz, D. Burgess, H. Lühr, R. L. Kessel, M. Dunlop, and C. J. Farrugia, Nonthermal ions and assotiated magnetic field behavior at a quasi-parallel Earth's bow shock, *J. Geophys. Res.*, *98*, 3889–3905, 1993.

Winske, D., and M. M. Leroy, Diffuse ions produced by electromagnetic ion beam instability, *J. Geophys. Res.*, *89*, 2673–2688, 1984.

Winske, D., and K. B. Quest, Electromagnetic ion beam instabilities: comparison of one- and two-dimensional simulations, *J. Geophys. Res.*, *91*, 8789, 1986.

Woodcock, J. P., Comment on Phase space evolution in linear instabilities, *Phys. Plasmas*, *2*, 4372, 1995.

P. Hellinger, Institute of Atmospheric Physics, Prague 14131, Czech Republic. (helinger@ufa.cas.cz)

A. Mangeney, Observatory of Paris, Meudon 92190, France. (mangeney@megasv.obspm.fr)